Journal of Solid State Chemistry **163,** 527–533 (2002)
doi:10.1006/jssc.2001.9442, available online at http://www.idealibrary.com on IDEAL®

Phase Analysis and Oxygen Storage Capacity of Ceria-Lanthana-Based TWC Promoters Prepared by Sol–Gel Routes

Francesca Deganello and Antonino Martorana[1]

Dipartimento di Chimica Inorganica, Universita' di Palermo, Viale delle Scienze, I-90128 Palermo, Italy and ICTPN-CNR, via Ugo La Malfa, 153, I-90146 Palermo, Italy

Received July 31, 2001; in revised form October 17, 2001; accepted October 26, 2001

Ceria–lanthana-based promoters of three-way catalysts are synthesized by two different sol–gel routes, involving nitrate precursors. The oxygen uptake ability of these compounds is measured by O_2 chemisorption. The specific surface area is determined by N_2 adsorption (BET). X-ray diffraction data are analyzed by Rietveld refinement, demonstrating that lanthanum forms solid solution with CeO_2; its total amount in ceria depends on the competitive formation of La–Al mixed oxides and on the synthetic method. The O_2 uptake ability is essentially determined by the La content in the ceria–lanthana solid solution, while it is independent on the surface area and on the CeO_2 particle size. The O_2 uptake ability increases with the La:Ce relative amount in the ceria–lanthana solid solution, but decreases beyond a La:Ce molar ratio greater than ≈ 0.18. This behavior is ascribed to the stable association of vacancy–vacancy or vacancy–dopant cation.

Key Words: **TWC catalyst; ceria; sol–gel; Rietveld refinement; oxygen storage capacity.**

1. INTRODUCTION

Ceria-based compounds are widely used as three-way automotive catalysts (TWC) for oxidation of CO and hydrocarbons and reduction of NO_x (1). Cerium oxide, due to the very low redox potential of the Ce^{4+}/Ce^{3+} couple ($E^0 = 1.7$ V), can take up oxygen from lean fuel gas and release it during fuel-rich operation. Owing to this property, usually designated as Oxygen Storage Capacity (OSC) (1), CeO_2-based promoters are able to bring the reaction mixture within the range of composition (the so-called stoichiometric window) that ensures the most effective conversion of the pollutants. The actual catalytic activity is carried out by the supported precious metals (2). Although the importance of ceria-based catalysts in automotive pollution control is nowadays well recognized, improvements are still pursued in order to enhance the activity during air-to-fuel ratio fluctuations, to improve the oxidation rate during cold start operations and to get better thermal stability and durability of the catalysts.

CeO_2 has a cubic fluorite-like structure in which cerium coordinates 8 oxygen anions at the corners of a cube, while oxygen is tetrahedrally surrounded by 4 cerium cations. It has been demonstrated that the OSC of cerium oxide is improved by suitable doping with different cationic species and in particular with lanthanum (2–4). In the solid solutions $Ce_{1-x}La_xO_{2-x/2}$, the neutrality of the lattice charge is ensured by the formation of one reticular oxygen vacancy every two La^{3+} substituting two Ce^{4+} cations; these defects improve the rate of exchange of oxygen with the environment by a mechanism of vacancy diffusion (4). The linear increase of the cell constant a_0 of $Ce_{1-x}La_xO_{2-x/2}$, observed for increasing x values (4, 5), is related to the larger radius of La^{3+} (1.16 Å) with respect to Ce^{4+} (0.97 Å) (6). *In situ* X-ray diffraction experiments (4) showed that a_0 in lanthanum-doped ceria undergoes expansion and contraction under alternating reduction and oxidation cycles, respectively. The phenomenon, originating from the larger ionic radius of Ce^{3+} (1.14 Å), demonstrates that the oxygen exchange and the related Ce^{4+}/Ce^{3+} transition concerns the bulk of the compound.

Currently, ceria-based systems are usually supported on transition aluminas, with the aim of achieving better dispersion of the active phase and improvement of the oxygen exchange rate. Lanthanum is able to stabilize transition aluminas toward the formation of the stable corundum phase, probably by the occupation of vacant octahedral sites in the Al_2O_3 spinel structure (7) or by the formation of a two-dimensional La–Al compound coating the support surface (8). Actually, a high thermal stability is an essential requirement for the CeO_2 containing supports, since in automotive applications the converter is close to the engine, and temperatures of about 1000°C can be reached. Only

[1]To whom correspondence should be addressed. E-mail nino@ictpn.pa.cnr.it.

0022-4596/02 $35.00

a limited number of studies are concerned with ceria–lanthana mixed oxides supported on alumina (2, 3, 9, 10). It is evident that the net result of combining La^{3+} with CeO_2 and Al_2O_3 is not easy to anticipate, due to the strong dependence of the structure and of the redox behavior on the employed synthetic route.

Materials with high surface area and good thermal stability are prepared by sol–gel methods (11, 12). In gel-based synthesis, the cations are molecularly mixed and spatially fixed in the gel, reducing diffusion distances during thermolysis and thus lowering the temperature for oxide formation. A paper (13) concerning the preparation of Ce–La–Al TWC catalysts by a sol–gel process involving heterometallic alkoxides was published some years ago. In the present paper, two inorganic sol–gel methods for obtaining a lanthanum-doped CeO_2 phase dispersed in an alumina matrix are described. Both techniques allow the introduction of all the oxide components (alumina, ceria, and lanthana) homogeneously and in a single step. With one of the two methods it is also possible to introduce a precious metal precursor simultaneously with the other components. The structural details of the mixed oxides prepared by these techniques are determined by Rietveld analysis, while the specific surface area is measured by N_2 physisorption using the BET method. The O_2 uptake ability at room temperature after reduction with H_2 is also determined and correlated with the microstructural features of the investigated compounds.

2. EXPERIMENTAL

2.1. Samples Synthesis

Two different sol–gel preparation routes have been applied, both starting from inorganic nitrate precursors, namely the citrate complex method (Cit) and the polyethyleneglycol method (PEG).

In the Cit method, equimolecular amounts of nitrate precursors and citric acid were dissolved in deionized water and subjected for 4 h to constant mechanical stirring at 80°C. During this phase of the synthesis, the complex citrates formed by substitution of nitrate ions with citrate ligands condensed together forming a gel. Then the solution was evaporated under vacuum until a gel was formed. Finally, the gel was evaporated under vacuum without stirring at 70°C for 24 h. In this way, after decomposition of the nitrate to nitrous oxides, a sponge solid was obtained that was calcined at 600°C for 4 h and for the same time at 1000°C.

The PEG method has been already used for the synthesis of ceramics (14) but it has not yet been used for automotive catalysts. At suitable PEG–nitrate ratios the PEG chains enclose the precursor molecules in a sort of micelle. An amount of PEG (MW = 20000), equal to the total moles of used precursors is dissolved in water: the solubility of PEG in water is 1g/10ml. When dissolution of PEG is completed, a solution of the nitrate precursors in deionized water is added. Water is evaporated at 80°C in an oil bath, until the formation of a dense gel. Then the oil bath temperature is increased to 158°C, giving rise to nitrate decomposition. After the gel is transformed to a solid powder, the bath temperature is increased to 182°C to decompose the PEG. The decomposed powder is then calcined to 600°C for 4 h and to 1000°C for 4 h. Several compounds were prepared by the Cit or the PEG method, with different amounts of aluminum, cerium, and lanthanum oxides. One PEG sample was prepared by adding a palladium precursor, to get PdO particles dispersed in the oxide matrix. Besides a commercial ceria (Aldrich, powder <5 micron, 99,9%, lot. no. 14728DR), also a pure CeO_2 sample was prepared as a further reference by the PEG procedure.

2.2. Samples Characterization

X-ray diffraction (XRD) measurements were carried out on a PHILIPS PW1830 X-ray powder diffractometer using Ni-filtered Cu$K\alpha$ radiation; the step size was 0.02° 2θ, between 5 and 10 times smaller than the FWHM of the observed diffraction peaks. The integration time was 3 s per step, and the scan range was from 10 to 140°2θ. The diffraction patterns were analyzed by Rietveld refinement using the GSAS package (15). Tchebischeff polynomials for the background and Pseudo-Voigt peak profile functions were used in the refinements. The best fitting procedure gave the structural parameters of the investigated compounds, and in particular the cell edge lengths and the relative phase compositions. The site occupancy factors of cerium and lanthanum in the ceria–lanthana mixed oxide were not refined because, differing by only one electron, these atoms are hardly distinguishable by X-rays.

The specific surface area has been determined by nitrogen gas adsorption at 77 K, using the BET method (Sorptomatic 1900, Carlo Erba Instruments). All samples were pretreated in vacuum at 350°C for 1 h and 30 min prior to the measurements.

The OSC of the investigated samples has been evaluated according to the method described in the literature (16) and involving the measurement of oxygen chemisorbed by the catalysts at room temperature. A conventional volumetric apparatus has been used, constituted by a U-shaped quartz reactor, a manometer for measuring the pressure, an oven connected to a temperature controller, and two vacuum pumps. The samples (100 mg) were prereduced in situ in a H_2 flow (35 ml/min) at 500°C for 2 h (temperature ramp: 17°C/min), and then left under vacuum for 1 h at 500°C. The amount of chemisorbed oxygen was calculated as mmol O per mol Ce.

3. RESULTS AND DISCUSSION

An outline of the synthesized samples and of the Ce, La, Al, and Pd molar compositions, as determined from the

TABLE 1

Elemental Molar % Composition Relative to the Four Elements Ce, La, Al and Pd, Determined from the Input Synthesis Amounts

Sample[a]	Ce	La	Al	Pd
CeO_2[b]	100	0	0	0
CeO_2–PEG[c]	100	0	0	0
CLAP1	20.2	8.0	71.9	0
CLAP2	12.0	4.5	83.5	0
CLAP3	5.3	2.1	92.7	0
CLAC1	20.1	7.9	72.0	0
CLAC2	36.8	24.2	39.0	0
CLP1	80.2	19.8	0	0
CLP2	71.2	28.8	0	0
PdCLAP[d]	18.8	8.0	71.9	1.3

[a] Key for the names: "C" for Cerium, "L" for Lanthanum, "A" for Aluminum, "P" for PEG, the second "C" for Cit.

[b] Purchased from Sigma–Aldrich.

[c] Prepared by the PEG method.

[d] Palladium nitrate added with the other oxide precursors.

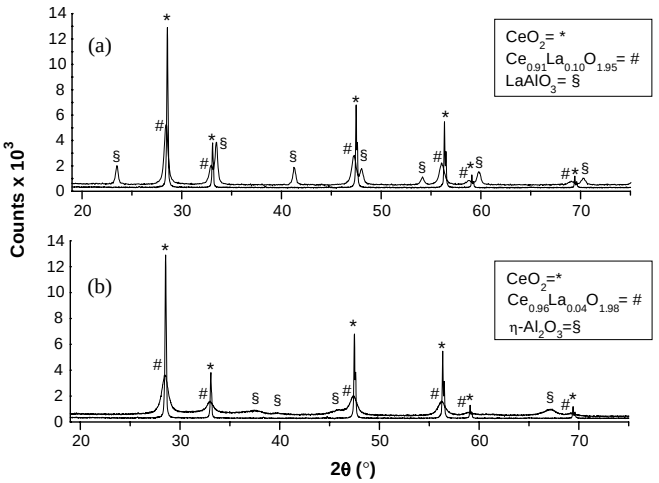

FIG. 1. Powder patterns of (a) CLAC2 and (b) CLAP3. As a reference, the scattering intensities (not to scale) of CeO_2–PEG are also plotted. The different phase components are indicated.

input preparation amounts, is given in Table 1. Since the exploited syntheses do not involve loss of reagents, the actual amounts should be very close to the nominal amounts. In fact, Ce, La, and Pd K-edge X-ray absorption experiments performed at the European Synchrotron Radiation Facility (ESRF) allowed to confirm this assumption by the analysis of the heights of the respective absorption jumps (F. Deganello, A. Longo, and A. Martorana, manuscript in preparation.). Most of the samples have a similar La:Ce molar ratio (La:Ce $\cong$ 0.4) and varying Al molar amount ranging from 0 (CLP2) to 92.7% (CLAP3). CLAC2 is richer in lanthanum (La:Ce $\cong$ 0.66) and CLP1 in cerium (La:Ce $\cong$ 0.25).

The diffraction patterns of the two CeO_2 samples show the typical peaks of the fluorite-like structure, with a reticular constant $a_0 = 5.4110$ Å, in fair agreement with the value reported in the literature for crystalline ceria (6). Figures 1a and 1b report two representative XRD patterns (relative to CLAC2 and CLAP3, respectively) and, superimposed for reference, the lines of CeO_2–PEG. Both sets of data indicate the presence of a ceria-like structure; however, the displacement of the peaks toward smaller 2θ angles with respect to the reference compound demonstrates that the cell constant is larger and, therefore, that doping of ceria with lanthanum is effective. The two patterns of Fig. 1 are different mainly because CLAC2 (Fig. 1a) shows the features characteristic of a perovskitic $LaAlO_3$ phase, while in CLAP3 (Fig. 1b) the presence of a transitional alumina, probably η-alumina (17), is more evident. According to the qualitative observations depicted in Fig. 1, the analysis of all the Al-containing samples was carried out by the simultaneous Rietveld refinement of the above cited ceria–lanthana, lanthanum aluminate, and η-alumina phases. The fittings relative to CLP1, CLAC2, and CLAP3 are drawn in Figs. 2–4, respectively, and the agreement factors for all the refinements are reported in Table 2.

Table 3 reports the percentage of molar phase composition and the a_0 values of the fluoritic phases determined by the Rietveld refinements. The La:Ce molar ratios of the fluoritic phases, also reported in Table 3, have been determined on the basis of the refined a_0 values and assuming, according to the Vegard's law, a linear dependence of a_0 on the La content. This behavior was observed on a wide composition range ($0 \leq x \leq 0.52$) by XRD and confirmed by lattice energy calculations (5). The Rietveld analysis performed on CLP1 and CLP2 demonstrated that two fluoritic structures are present, with different cell constants a_0 and, therefore, different lanthanum concentrations. Similar phase separation was observed also by other authors in samples of La-doped ceria obtained either by hydrothermal (18) or by sol–gel (19) synthesis. It is possible that the phase separation can take place through a diffusion process that is feasible in sol–gel processes. In Fig. 2b the well-resolved contributions from the two phases are evident. The overall calculated molar ratios La:Ce for CLP1 (La:Ce = 0.28) and CLP2 (La:Ce = 0.49) are in satisfactory agreement with the input quantities (see Table 1).

From inspection of Tables 1 and 3 it is clear that, except for CLP1 and CLP2, only a small part of the input lanthanum is dissolved in ceria and that the PEG route seems to be more effective than Cit for the solid solution formation. In CLAC2 (see Figs. 3a and 3b) the formation of a substantial amount of lanthanum aluminate is manifest. All the other aluminum-containing samples show the presence of a minor quantity of $LaAlO_3$, not recognizable at all

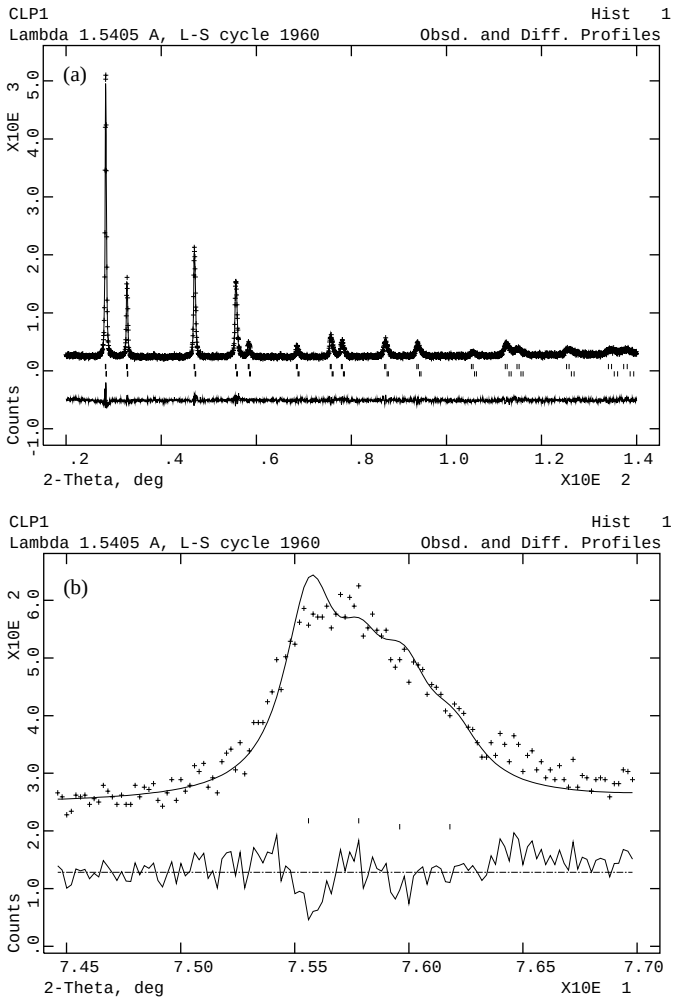

FIG. 2. Observed powder pattern of (crosses) CLP1, (solid line) fitted intensity, and difference curve resulting from the Rietveld refinement. Two fluoritic phases with different La content are present and indicated by, respectively, the upper and lower series of thick marks. In (a), the total pattern is shown; in (b) the enlargement in the 74.5–77° 2θ shows the well-resolved contributions from the respective Cu$K\alpha_1$–$K\alpha_2$ lines of the two phases.

in CLAC1, and of η-Al_2O_3. Concerning this latter phase, it should be remarked that the fitting is not completely satisfactory, although somewhat better than the agreement achieved with the more common γ-phase, belonging to the same *Fd*3*m* space group but having different Al positions (17). In particular, in the worst fitting interval 34–44°2θ (see Fig. 4b) the calculated peaks are shifted, in opposite directions, of about 0.03° 2θ from the experimental peaks. It is well known that structural disorder affects transitional aluminas (17, 20), producing problems in the Rietveld refinements; in our case included lanthanum could be a further source of disorder, giving rise also to the amorphous halo in the range 28–42° 2θ (see Fig. 4a), fitted by the use of Tchebischeff polinomials. The consideration that a noteworthy La amount cannot be recovered by the Rietveld analyses performed on the Al-containing samples and that the amount of lanthanum dissolved in ceria decreases as the input Al quantity is increased could provide a further indication of the formation of lanthana–alumina solid solution. In conclusion, it is likely that sol–gel synthesis allows the competitive formation of different La-containing phases, in relative amounts depending on the probability that the respective oxide components come into contact with each other. As already found in the literature (9) and confirmed by EXAFS experiments (F. Deganello, A. Longo, and A. Martorana, manuscript in preparation), the formation of cerium aluminate is inhibited in the presence of lanthanum. The formation of a surface La–Al compound coating the

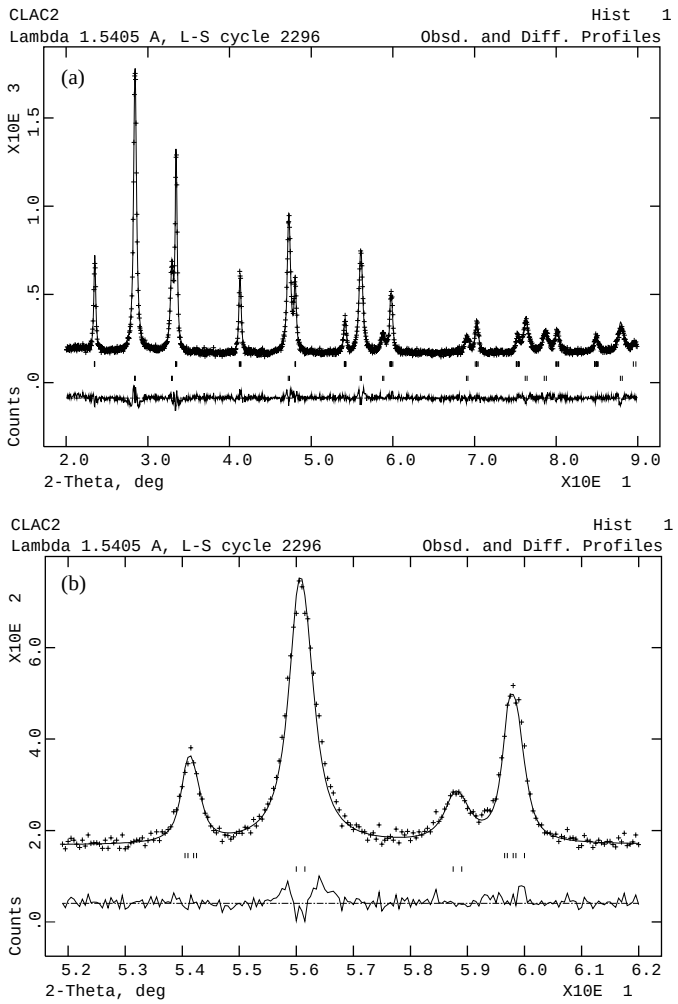

FIG. 3. Observed powder pattern of (crosses) CLAC2, (solid line) fitted intensity, and difference curve resulting from the Rietveld refinement. The upper and lower series of thick marks are relative to the lanthanum aluminate and, respectively, to the ceria lanthana phase. In (a), the total pattern is shown; in (b) the enlargement relative to the 52–62° 2θ shows contributions to the total intensity from both phases.

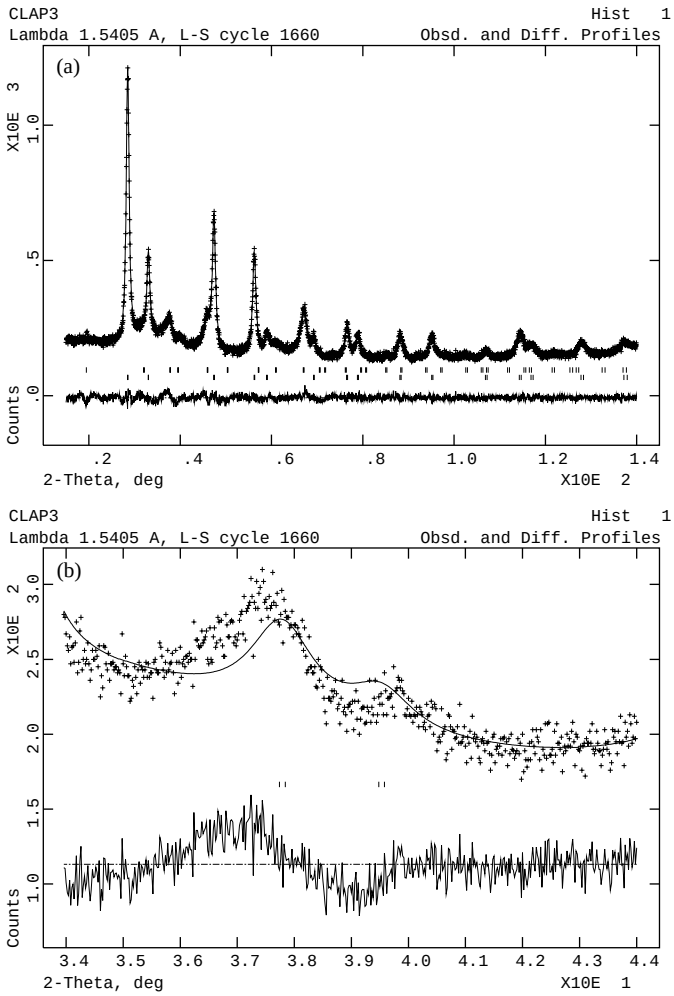

FIG. 4. Observed powder pattern of (crosses) CLAP3, (solid line) fitted intensity, and difference curve resulting from the Rietveld refinement. The upper and lower series of thick marks are relativeto η-alumina and, respectively, to the ceria lanthana phase. In (a) the total pattern is shown; the enlargement reported in (b) points out the misfit in the 34–44° 2θ range.

alumina domains (8) cannot be excluded but, of course, cannot be evidenced by XRD.

The specific surface areas determined by BET are reported in Table 4 and are in agreement with the values reported in the literature for similar systems (4). The crystallite size of the fluoritic phase, determined by the Scherrer equation, and the OSC values are also reported for all the investigated samples. It is clear, from the analysis of these parameters, that the OSC is not substantially improved by small particle size or high specific surface area. With this respect, it is interesting to note that the particle size of CLAC2 is twice that of CLAC1 (but the OSC is larger) and that the surface area of CLAP1 (OSC = 98) is smaller than that of CLAP3 (OSC = 16). Morris *et al.* (5) found by lattice energy calculations that the interaction between dopant La^{3+} and anion vacancy is weak (about 0.2 eV), suggesting

TABLE 2
Agreement Factors[a] for the Rietveld Refinements Performed on the Investigated Samples

Sample	*R*wp	*R*p	Ddw	χ^2
CeO_2	4.49	3.58	1.96	0.73
CeO_2–PEG	7.09	5.30	1.14	1.89
CLAP1	5.14	4.08	1.20	0.59
CLAP2	4.93	3.91	1.33	0.49
CLAP3	4.77	3.74	1.46	0.46
CLAC1	6.10	4.81	1.78	1.12
CLAC2	5.25	4.16	1.45	0.66
CLP1	6.80	5.39	1.39	1.46
CLP2	6.29	4.95	1.54	1.32
PdCLAP	7.40	5.81	1.12	1.81

[a] $Rwp = 100(\sum w(I_o - I_c)^2/\sum wI_o^2)^{-1/2}$; $Rp = 100(\sum|I_o - I_c|/\sum I_o)$; $Ddw = \sum_{i=2,N}[(I_o - I_c)_i/\sigma_i - (I_o - I_c)_{i-1}/\sigma_{i-1}]^2/\sum_{i=1,N}[(I_o - I_c)_i/\sigma_i]^{-2}$; $\chi^2 = \sum w(I_o - I_c)^2/[N_{obs}\text{-}N_{var}]$.

that the oxygen vacancies are not bound to the dopant cations, and O'Neill *et al.* (21) gave experimental evidence to this hypothesis demontrating the oxygen mobility in La-doped ceria by ^{139}LaMASNMR. The in situ X-ray diffraction experiments performed by Ozawa *et al.* (4) confirmed this result, showing that the exchange of oxygen with the environment involves the bulk of the ceria–lanthana mixed oxide. It is therefore clear that the mobility of oxygen in the ceria–lanthana matrix, achieved through a mechanism of vacancy diffusion, is the most important parameter for OSC and that morphological parameters, at least in the investigated range of values, are less relevant in this respect. This conclusion is in agreement with the findings of other authors relative to CeO_2–La_2O_3 (22, 23) mixed oxides systems. Therefore, it is likely to conclude that the OSC depends mostly on the content of lanthanum in ceria.

In Fig. 5 the OSC of the investigated samples, as mmol O per mol Ce, is plotted *vs* the La:Ce molar ratio in the ceria–lanthana solid solution. The two phases of CLP1 and CLP2 are discriminated by weighting the partial contributions to the overall OSC by the respective molar amounts, as determined from the Rietveld refinements. The OSC of the first component of CLP1 (La:Ce = 0.20) is assumed to be almost equal to that of CLAP1 (showing a similar La:Ce ratio) and allows to determine the OSC of the second component, having La:Ce = 0.33, as 56 mmolO/molCe. A similar procedure allows to discriminate the contribution to the total OSC of the first component of CLP2 (assumed to be equal to 56 mmolO/molCe as the La:Ce ratio is nearly equal to the above reported value of 0.32) from the OSC of the second component (reported in Fig. 5 in correspondence to the composition La:Ce = 0.52).

From inspection of Fig. 5, it is evident that a maximum in the OSC takes place, so that it seems quite possible that the highest OSC is obtained in correspondence of an optimal

TABLE 3
Results of the XRD Analysis

Sample	PdO[a]	$\eta - Al_2O_3$[a]	$LaAlO_3$[a]	$Ce_{1-x}La_xO_{2-x/2}$[a,b]	a_0(Å)[c]	La/Ce[d]
CeO_2	—	—	—	100	5.4105(1)	0
CeO_2–PEG	—	—	—	100	5.4108(1)	0
CLAP1	—	51(1)	2.2(6)	46.4(6)	5.4569(1)	0.17
CLAP2	—	73.4(5)	0.5(1)	26.1(1)	5.4484(1)	0.13
CLAP3	—	88(1)	~ 0	12.3(3)	5.4245(1)	0.05
CLAC1	—	62.2(3)	—	37.8(1)	5.4361(4)	0.09
CLAC2	—	—	36.1(2)	63.9(2)	5.4406(2)	0.10
CLP1[e]	—	—	—	33.0(8)	5.4636(2)	0.20
				67.0(4)	5.4889(1)	0.33
CLP2[e]	—	—	—	16.8(8)	5.4864(5)	0.32
				83.2(1)	5.5188(1)	0.52
PdCLAP	3(1)	48(1)	4.9(1)	44.3(1)	5.4509(2)	0.15

[a]mol% of the phase detected by XRD. The errors are reported in parentheses. Due to the very small amount of $LaAlO_3$ in CLAP3, the uncertainty in the refined value retrieved by GSAS is very large, about 100%.
[b]Fluorite-like phase $Ce_{1-x}La_xO_{2-x/2}$; $x = 0$ in the pure ceria samples.
[c]Cell edge length of the fluoritic phase.
[d]La/Ce molar ratio $(x/1-x)$ in the fluoritic phase $Ce_{1-x}La_xO_{2-x/2}$.
[e]Two fluoritic phases were detected, with the reported phase amounts, a_0 and La/Ce molar ratios.

amount of dissolved lanthanum. The rise of the OSC for increasing dopant concentration is dependent on the number of oxygen vacancies that affects the oxygen mobility within the ceria network. Beyond the limit of about 0.18 for the La:Ce molar ratio, the decrease of the OSC could be due to an excess density of vacancies, leading to stable vacancy–dopant cation association (24–26) that limits the number of mobile vacancies and therefore the ability of the compound of exchanging oxygen with the environment. Several papers concerning the anionic conductivity in trivalent rare earth (RE)-doped ceria (18, 24, 27) give experimental evidence that the ionic conductivity actually starts to decrease at about $x/(1-x) = 0.18$ in $Ce_{1-x}RE_xO_{2-x/2}$, confirming that in these systems the mobility of oxygen is crucially dependent on the optimal amount of dopant species. The deviation of the OSC of PdCLAP from the general behavior is not surprising, since the activating action of the precious metal is well documented (2).

TABLE 4
Chemisorption Results, Particle Size of the Ceria Phase, and Specific Surface Area of the Investigated Samples

Sample	O_2 chemisorption (mmolO/mol Ce)	XRD Particle size[a] (Å)	BET Surface area[b] (m^2/g)
CeO_2	7.6	506	10
CeO_2–PEG	0.1	1108	0.8
CLAP1	98	154	19
CLAP2	34	126	9
CLAP3	16	112	29
CLAC1	15	93	10
CLAC2	25	208	6
CLP1	70	348	6
		380	
CLP2	32	252	6
		375	
PdCLAP	88	186	17

[a]Determined by the Scherrer's equation, taking into account the instrumental broadening. The error is estimated as ±5%.
[b]The error is estimated as ±10%.

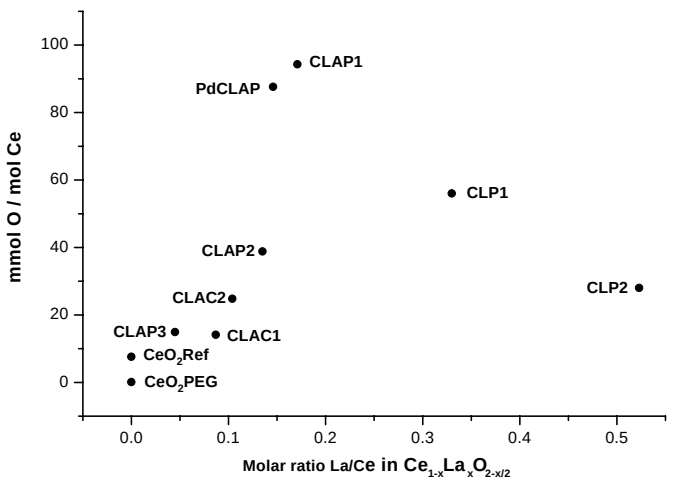

FIG. 5. Oxygen storage capacity (in mmol O/ mol Ce) as a function of the molar ratio $x/(1-x)$ in the investigated samples.

4. CONCLUSION

Two different sol–gel routes, using citric acid and polyethylene glycol as gelling agents, have been used to prepare Ce–La–Al mixed oxides in a single step, and, in one case, to obtain Pd particles dispersed in the oxide matrix. The Cit procedure seems to be less effective in producing ceria–lanthana solid solutions with a high dopant concentration. The presence of aluminum determines in both synthesis routes the competitive formation of a La–Al mixed oxide that in some cases is clearly revealed by XRD as a stoichiometric compound. On the basis of the evaluation of the total lanthanum amount detected by XRD, it has been argued that a substantial quantity is dissolved in the alumina matrix.

An analysis of the OSC of the investigated compounds, led to the conclusion that this parameter is crucially dependent on the La:Ce molar ratio in the ceria–lanthana solid solution, and that other parameters such as the surface area and the crystallite size, at least in the investigated range of variation of these parameters, are not relevant. The maximum of oxygen storage capacity evidenced in correspondence of La:Ce$\cong$0.18 in the ceria–lanthana lattice corresponds fairly well to the observed decrease of ionic conducibility in CeO_2 doped with trivalent lanthanides, confirming that both phenomena are mainly ruled by the mobility of oxygen vacancies.

ACKNOWLEDGMENTS

This study was performed with the financial support of the MURST project MM03267484_002. The authors thank R. Prins of ETH Zurich for advice and stimulating discussion.

REFERENCES

1. A. Trovarelli, *Catal. Rev. Sci. Eng.* **38**(4), 439–519 (1996).
2. T. Miki, T. Ogawa, M. Haneda, N. Kakuta, A. Ueno, S. Tateishi, S. Matsuura, and M. Sato, *J. Phys. Chem.* **94,** 6464–6467 (1990).
3. R. K. Usmen, G. W. Graham, W. L. H. Watkins, and R. W. McCabe, *Catal. Lett.* **30,** 53–63 (1995).
4. M. Ozawa and C.-K. Loong, *Catal. Today* **50,** 329–342 (1999).
5. B. C. Morris, W. R. Flavell, W. C. Mackrodt, and M. A. Morris, *J.Mater. Chem.* **3,** 1007–1013 (1993).
6. S. J. Hong and A. V. Virkar, *J. Am. Ceram. Soc.* **78,** 433–439 (1995).
7. L. J. Alvarez, J. P. Jacobs, J. F. Sanz, and J. A. Odriozola, *Solid State Ionics* **95,** 73–79 (1997).
8. A. Galtayries, G. Blanco, G. A. Cifredo, D. Finol, J. M. Gatica, J. M. Pintado, H. Vidal, R. Sporken, and S. Bernal, *Surf. Interf. Anal.* **27,** 941–949 (1999).
9. G. W. Graham, P. J. Schmitz, R. K. Usmen, and R. W. McCabe, *Catal. Lett.* **17,** 175–184 (1993).
10. D. H. Kim, S. I. Woo, J. M. Lee, and O. B.Yang, *Catal. Lett.* **70,** 35–41 (2000).
11. M. Kakihana, *J. Sol–Gel Sci. Technol.* **6,** 7–55 (1996).
12. M. A. Cauqui and J. M. Rodriguez-Izquierdo, *J. Non-Cryst. Solids* **147–148,** 724–738 (1999).
13. C. K. Narula, W. H. Weber, J. Y. Ying, and L. F. Allard, *J. Mater. Chem.* **7,** 1821–1829 (1997).
14. X. H. Liu, J. Yang, L. Wang, X. J. Yang, L. D. Lu, and X. Wang, *Mat. Sci. Eng. A* **289,** 241–245 (2000).
15. A. C. Larson and R. B. von Dreele, "GSAS, the General Structure Analysis System." Los Alamos National Laboratory, 1991.
16. H. C. Yao and Y. F. Yu Yao, *J. Catal.* **86,** 254–265 (1984).
17. R.-S. Zhou and R. L. Snyder, *Acta Crystallogr. Sect. B* **47,** 617–630, (1991).
18. S. Dikmen, P. Shuk, and M. Greenblatt, *Solid State Ionics* **126,** 89–95 (1999).
190. P. G. Harrrison, A. Kelsall, and J. V. Wood, *J. Sol–Gel Sci. Technol.* **13,** 1049–1055 (1998).
20. I. Levin and D. Brandon, *J. Am. Ceram Soc.* **81,** 1995–2012 (1998).
21. W. M. O'Neill and M. A. Morris, *Chem. Phys. Lett.* **305,** 389–394 (1999).
22. M. O'Connell and M. A. Morris, *Catal. Today* **59,** 387–393 (2000).
23. E. Mamontov, T. Egami, R. Brezny, M. Koranne, and S. Tyagi, *J. Phys. Chem. B* **104,** 11110–11116 (2000).
24. T. Ohashi, S. Yamazaki, T. Tokunaga, Y. Arita, T. Matsui, T. Harami, and K. Kobayashi, *Solid State Ionics* **113–115,** 559–564 (1998).
25. L. Minervini, M. O. Zacate, and R. W. Grimes, *Solid State Ionics* **116,** 339–349 (1999).
26. T. Norby, *J. Mater. Chem.* **11,** 11–18 (2001).
27. H. Yamamura, E. Katoh, M. Ichikawa, K. Kakinuma, T. Mori, and H. Haneda, *Electrochemistry* **68,** 455–459 (2000).